The Effects of Geometrical Parameters on Synaptic Transmission: A Monte Carlo Simulation Study

Piotr J. Kruk,* Henri Korn,# and Donald S. Faber*
Department of Neurobiology and Anatomy, Allegheny University of the Health Sciences, Philadelphia, Pennsylvania 19129 USA, and #Laboratory of Cellular Neurobiology, INSERM U261, Institut Pasteur, 75724 Paris Cedex 15, France

ABSTRACT Monte Carlo simulations of transmitter diffusion and its interactions with postsynaptic receptors have been used to study properties of quantal responses at central synapses. Fast synaptic responses characteristic of those recorded at glycinergic junctions on the teleost Mauthner cell (time to peak ~0.3–0.4 ms and decay time constant ~3–6 ms) served as the initial reference, and smaller contacts with fewer postsynaptic receptors were also modeled. Consistent with experimental findings, diffusion, simulated using a random walk algorithm and assuming a diffusion coefficient of 0.5–1.0 $\times$ 10^{-5} cm^2 s^{-1}, was sufficiently fast to account for transmitter removal from the synaptic cleft. Transmitter-receptor interactions were modeled as a two-step binding process, with the double-bound state having opened and closed conformations. Addition of a third binding step only slightly decreased response amplitude but significantly slowed both its rising and decay phases. The model allowed us to assess the sources of response variability and the likelihood of postsynaptic saturation as functions of multiple kinetic and spatial parameters. The method of nonstationary fluctuation analysis, typically used to estimate the number of functional channels at a synapse and single channel current, proved unreliable, presumably because the receptors in the postsynaptic matrix are not uniformly exposed to the same profile of transmitter concentration. Thus, the time course of the probability of channel opening most likely varies among receptors. Finally, possible substrates for phenomena of synaptic plasticity, such as long-term potentiation, were explored, including the diameter of the contact zone, defined by the region of pre- and postsynaptic apposition, the number and distribution of the receptors, and the degree of vesicle filling. Surprisingly, response amplitude is quite sensitive to the size of the receptor-free annulus surrounding the receptor cluster, such that expansion of the contact zone could produce an appreciable increase in quantal size, normally attributed to either the presence of more receptors or the release of more transmitter molecules.

INTRODUCTION

Recent studies on the properties of central synapses, particularly on those of single quanta, have raised a number of questions that are difficult to resolve on the basis of experimental data alone, due to technical or theoretical limitations. For example, the amplitude and kinetics of the miniature postsynaptic currents (mPSCs) or single synaptic quanta recorded from a single target neuron often display a high degree of variability (Bekkers et al., 1990; Bekkers and Stevens, 1995; Frerking et al., 1995) regardless of whether they are generated by relatively few or many synapses (Lewis and Faber, 1996; Liu and Tsien, 1995a,b). It is not clear whether this variability is intrinsic to the individual synapses or rather is due to differences within an ensemble of contacts, each of which alone produces more stereotyped responses. On the one hand, it has been suggested that, as with the neuromuscular junction, an increase in the amount of transmitter released from a synaptic vesicle produces a larger quantal current, that is, that the postsynaptic receptors are reliable detectors of the amount of transmitter released (Frerking et al., 1995; Bekkers et al., 1990). At the other extreme, data from some central junctions have been interpreted as indicating quantal responses in the central system are invariant, due to all or a fixed fraction of the synaptic channels being open at the peak of the mPSC. The *latter* alternative presumes a saturated response, a condition most likely met when there are few (<100) postsynaptic receptors and a relatively large number of transmitter molecules packaged in a vesicle. However, even saturated binding does not exclude variance, since the stochastic properties of activated channels necessarily introduce some variability (Faber et al., 1992). While this and other related issues (role of the degree of vesicle filling, and the contributions of other pre and postsynaptic factors to quantal waveform, amplitude, and variability) have been the focus of most studies, it is surprising that effects of synaptic geometry, which is well known, have been overlooked. In this work we address each of these *issues*, using modeling techniques that are described below and allow insight into the microstructural design of single synapses.

Simulations of quantal synaptic responses have been utilized by a number of investigators, beginning with the initial attempts by Eccles and Jaeger (1958) to model the neuromuscular junction. The physical and chemical processes of synaptic transmission, including transmitter diffusion and interactions with postsynaptic receptors, can be treated as analytical functions of time and space. Indeed, the initial models connecting these processes were analytical, that is, solutions to a series of simultaneous differential equations (Land et al., 1981, 1984; Wathey, 1979; Faber et al., 1985; Busch and Sakmann, 1990), and they provided insights

Received for publication 9 April 1997 and in final form 5 September 1997.
Address reprint requests to Donald S. Faber, Ph.D., Department of Neurobiology and Anatomy, Allegheny University of the Health Sciences, 3200 Henry Avenue, Philadelphia, PA 19129. Tel.: 215-842-4600; Fax: 215-843-9082; E-mail: dfaber@ccc.medcolpa.edu.

0006-3495/97/12/2874/17 $2.00

relative to the size and time course of an average or "typical" response, without providing information about biophysical variations. This limitation can be overcome with Monte Carlo models, which treat diffusion probabilistically and assign probabilities to all state transitions (Bartol et al., 1991). A few such stochastic models of single synapses have been developed and tested (Bartol et al., 1991; Faber et al., 1992; Wahl et al., 1996; Blum and Idiart, 1994; Stiles et al., 1996). The initial model of the neuromuscular junction by Bartol et al. (1991) is particularly noteworthy since it established the methodology and thus provides a starting point for our approach. We have expanded it by incorporating the quite different structural features of central synapses.

A recent study focused on matching the properties of excitatory responses in the hippocampus using published rate constants, and then explored the effects of changing parameters such as temperature and the diffusion constant, and modeled the release process itself (Wahl et al., 1996). We have taken a different approach. Our interest initially centered on inhibitory responses mediated by glycine, particularly at synapses on the teleost Mauthner cell. In this case, the rate constants are not yet established, and it is necessary to explore their likely range. When these synapses were first simulated analytically, following the approach of Land et al. (1984) for the neuromuscular junction, the results already pointed to clear differences with that system (Faber et al., 1985). For example, it was predicted that due to the restricted size of the receptor cluster, down-regulation of receptor density would not alter the rise time of the mPSC, while at the neuromuscular junction it slows the rising phase of the response (Land et al., 1981), and this prediction was confirmed experimentally (Faber et al., 1985). This suggested that the design of central synaptic contacts, with a localized receptor matrix, imposes constraints not found in the periphery. Similarly, the first iteration of the Monte Carlo model of these synapses indicated that stochastic channel properties contribute significant intrinsic variability to their quantal currents, and again this conclusion was confirmed experimentally (Faber et al., 1992, 1995).

We have now expanded this analysis to study the effects of several geometrical parameters, such as the size of a synaptic contact, including the receptor cluster and receptor-free annulus surrounding it, on quantal size and kinetics. The results indicate that these factors are critical for quantal shape and size, and may contribute to long-term modifications in synaptic strength. These findings, part of which have been presented earlier in abstract form (Kruk and Faber, 1995), can now be explored with this model at junctions using other transmitters in the CNS. An unexpected outcome of our investigations is that nonstationary fluctuation analysis, often used to extract data about single channel conductance and number at synapses (Robinson et al., 1991; deKoninck et al., 1992; Traynelis et al., 1993), can be misleading.

METHODS

Two major processes were simulated for a single synaptic contact: 1) diffusion of transmitter in the synaptic cleft, and 2) the reactions (both chemical and conformational) of the postsynaptic receptor-channel complexes, referred to here as simply receptors or channels.

Two different algorithms were used. Initially, transmitter diffusion was simulated as in Faber et al. (1992), using a three-dimensional matrix that subdivided the synaptic cleft into multiple layers of small rectangular solids. At each discrete time step, the molecules from within a given solid could travel randomly, with a Gaussian distribution, into surrounding solids. Then the new numbers (destination) of transmitter molecules in each solid were calculated without storing information about individual trajectories. Some solids in the layer closest to the postsynaptic membrane were apposed to (i.e., contained) receptor molecules, each with a defined number of binding sites. The numbers of transmitter molecules in these solids were translated into local concentrations which in turn drove the receptor reactions, namely binding and channel gating, with the number of open channels being directly proportional to the postsynaptic current. This scheme correctly reproduced the dynamics of miniature glycinergic postsynaptic currents and provided predictions about the effects of varying receptor density and the number of transmitter molecules per vesicle. It also allowed exploration of the range of rate constants that produced responses having kinetics similar to those of glycinergic inhibitory postsynaptic currents (IPSCs) recorded from the goldfish Mauthner cell soma (see Results), as these IPSCs served as the starting or reference point for this research (Faber and Korn, 1980, 1982). However, the computational efficiency of that earlier algorithm was too low, because of unnecessary scanning of many spatial locations (grid points) which frequently contained no transmitter molecules.

The new version is more efficient because the positions of individual transmitter molecules are stored while the local concentrations, which often are zero, are not. Second, diffusion is now modeled using a random walk method (see below), with smaller time steps than used for simulating the kinetic interactions. Finally, the number of layers in the synaptic cleft is reduced to one, a modification favored by the relationship between the values of the diffusion coefficient and the thickness of the synaptic cleft. That is, diffusion is so fast and the cleft so narrow that the diffusion radius ($2\sqrt{Dt}$) would exceed cleft height within the first one or two time steps of the simulation, and thus the transmitter would be evenly distributed in that time. This reduction to a two-dimensional model also increases efficiency.

The initial algorithm was used for analyzing synapses with stereotyped geometry, but once it was determined that the new formulation produces essentially the same output (e.g., results of Faber et al., 1992), it was used to refine and expand the earlier predictions. The remainder of this Methods section describes this new algorithm in detail.

Contact zone and the receptor disk

The structure of a synapse encompasses a presynaptic release site, the synaptic cleft, and the postsynaptic receptor matrix. The cleft is treated as a flat cylinder between two circular surfaces representing the pre- and postsynaptic membranes (Fig. 1 *A*), and its radius defines the extent of the contact zone, $r_{contact}$. The postsynaptic receptors are also distributed within a smaller disk with a radius, $r_{disk} < r_{contact}$. This configuration is consistent with electron microscopic images of central synapses (Triller and Korn, 1982; Peters et al., 1991), where the contact zone may extend appreciably beyond the region delineated by the apposing postsynaptic density (PSD). The latter in turn is often associated with the receptor matrix, which may be slightly larger than the PSD but generally does not encompass the full contact zone (for example, see Faber et al., 1985). The receptor disk can be located anywhere within the postsynaptic membrane, although it is usually concentric with the contact zone, with its center apposed to the presynaptic release site. In this study, we tested contact radius values from 25 to 1600 nm.

The synaptic cleft is organized in a regular network of rectangular solids arranged in a single layer (Fig. 1 *B*). They have square bases, and their

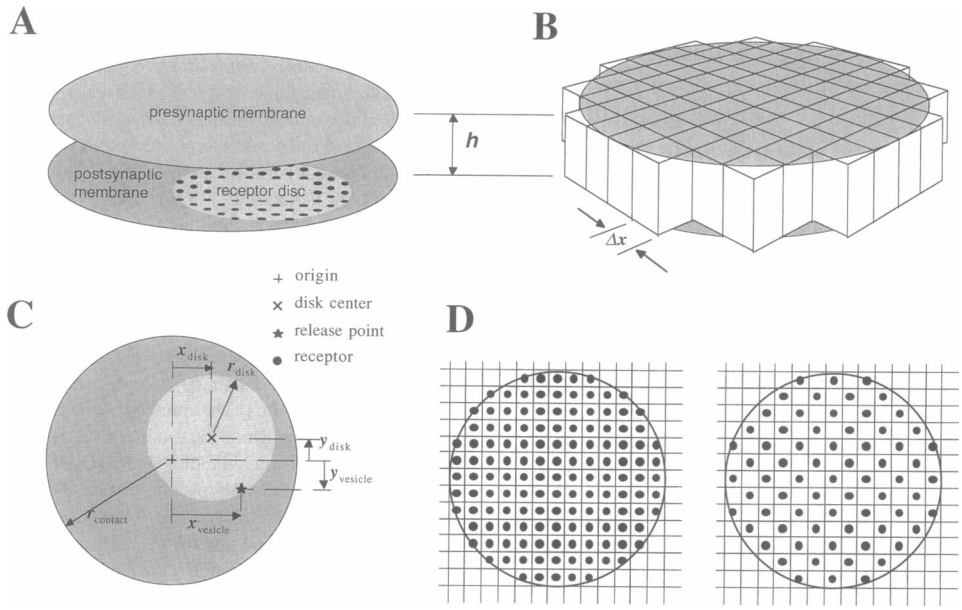

FIGURE 1 Schematic representation of the synapse. (*A*) Synapse represented by two parallel circular membranes, pre and postsynaptic, separated by the thickness of the synaptic cleft, *h*. (*B*) The cleft is divided into rectangular blocks (*solids*) arranged in a single layer. The blocks have a square base with the length of the sides, Δx, adjustable from 5 to 7.071 nm. Their total number depends on the radius of the contact zone. (*C*) View of the postsynaptic membrane. The larger circle represents the contact zone, its center marked with a plus (+), and the inner disk contains the receptors. The projection of a transmitter release point is marked with an asterisk (*). The disk center and the release site may be displaced from the center of the contact zone by the vectors $[x_{disk}, y_{disk}]$, and $[x_{vesicle}, y_{vesicle}]$, respectively ($r_{disk}$ and $r_{contact}$ defined in text). (*D*) Arrangement of receptor molecules within the receptor disk depends on their density. Each square of the grid represents one block. Two arrangements are shown: a receptor in every block within the receptor disk (i.e., density = $(\Delta x)^{-2}$, *left panel*); a receptor in every other block (i.e., density = $0.5(\Delta x)^{-2}$, *right panel*). Also possible are arrangements with receptors in every 4th, 8th, 16th block, etc., up to every 1024th block (not shown). Together with adjustment of Δx, this allows receptor density to assume values from 20 to 40,000 receptors per μm^2.

heights equal the distance between the two membranes (*h*, Fig. 1, *A* and *B*), usually 20 nm in this study.

The positions of the receptors and the transmitter molecules are defined by the solid they occupy. The solids are treated as points on a two-dimensional grid, with the program storing the position of molecules with an accuracy limited to point separation, thus neglecting their location within the solids. Similarly, the paradigm for modeling transmitter-receptor interactions neglects the position of a molecule within a solid when calculating its probability of interaction with a receptor (see Methods: Kinetics section). Each solid contains at most one receptor and any number of transmitter molecules. The dimensions of the solids and base (grid spacing, Δx) is determined by the program once the surface density of the receptors is defined (see below).

Receptor distribution

The receptors are evenly spaced in their disk, with its size = r_{disk} and its position relative to the center of the contact zone defined by x_{disk}, y_{disk} (Fig. 1 *C*). Thus, the disk is concentric with the contact zone if both x_{disk} and y_{disk} equal zero, which was the case for the results reported here. The density of the receptors, σ, can range from 200 to 40,000 μm^{-2}, and the program models it by adjusting 1) their distribution among the solids, so that they are regularly arrayed within a fraction of the solids (Fig. 1 *D*), and 2) the length Δx. This two-step approach first roughly changes density by a power fraction of 2, and then sets it more precisely by scaling Δx by a factor ranging from 1 to $\sqrt{2}$. In our simulations Δx ranged from 5 to 7.071 nm. The maximum density, 40,000 μm^{-2}, is achieved when one receptor occupies every solid, the minimum size of which is 5 nm. This upper limit is excessive, as it implies a receptor surface area no larger than 25 nm^2, and it was not used. While σ can be reduced to 20,000 μm^{-2} by simply doubling the surface of the base alone, any further dilution requires a change in receptor distribution.

Transmitter release and removal

Exocytosis is approximated with the instantaneous placement of a predefined number of molecules in a solid apposing the presynaptic "release site." The position of this site ($x_{vesicle}$, $y_{vesicle}$ in Fig. 1 *C*) and the number of molecules released can also be varied. Although we previously explored the effect of "off-center" release on response variability (Faber et al., 1992; see also Uteshev and Pennefather, 1996), the results described here all pertain to "on-center" release. That is, the release site position was (0, 0) and centered with x_{disk} and y_{disk}. Diffusion spreads the quantal packet throughout the contact zone, and some molecules will reach the receptors. When transmitter reaches the border of the contact zone, it has a 75% chance of remaining in the synapse per each diffusion time step (see below), only disappearing from the simulation when it diffuses through the circumferential opening. There is no other mechanism for removing transmitter, such as uptake, as diffusion alone appears sufficient at Mauthner cell inhibitory synapses (Titmus et al., 1996).

Random walk diffusion

Diffusion is modeled as a random walk process (Stibitz, 1969; Press et al., 1992), with each transmitter molecule moving in the *x* and *y* dimensions independently of other molecules. That is, during every time step (Δt) a molecule twice moves the distance of $\Delta x/2$, randomly in either the positive or negative direction. Consequently, it ends up in one of three locations, with a 50% chance to remain at its initial site, and a 25% chance to land

in the next solid in either direction (Fig. 2). The same process occurs in the y direction as well. After a large number of time steps, the probability of finding the molecule at any grid point in space will approach a Gaussian distribution centered around the point of departure (Fig. 2), and overall the transmitter spreads in the xy plane with an effective diffusion coefficient D.

$$D = \frac{(\Delta x)^2}{4\Delta t} \tag{1}$$

To assure that D has the value specified by the user, Δt is calculated directly from Eq. 1. For example, with the most often used value of 5×10^{-6} cm^2/s, and with Δx = 5–7.071 nm, Δt is on the order of 20 ns.

Kinetics

As in all similar models, the receptors (R) undergo both binding and unbinding of agonist (A), and the associated channels open or close. The rates of these reactions are designated by k_{+j} for binding, k_{-j} for unbinding, β for opening, and α for closing, where $+j$ designates the forward transition to the jth bound state, and $-j$ the backward transition from that state. The adopted model requires that these constants be converted into transition probabilities (P).

Since the typical diffusion time step Δt is very short (~20 ns), a longer, more reasonable time step δt (40–500 ns), which yields significant, albeit small, transition probabilities, is used for calculating the receptor reactions. It is adjusted automatically at the beginning of the simulation so that the transition probabilities do not exceed a preset maximum (0.0625 for the present simulations). Then, the transition probabilities in a single time step δt are:

for closing a channel

$$P_\alpha = 1 - \exp(-\alpha \times \delta t), \tag{2}$$

for opening a channel

$$P_\beta = 1 - \exp(-\beta \times \delta t), \tag{3}$$

and for unbinding

$$P_u = 1 - \exp(-k_{-j} \times \delta t). \tag{4}$$

With a single free molecule in the solid, the probability of binding is

$$P_{b1} = 1 - \exp(-k_{+j} \times \delta t \times c_1) \tag{5}$$

where c_1 is the concentration of one molecule in the solid. With m molecules it becomes equal to

$$P_{bm} = 1 - (1 - P_{b1})^m. \tag{6}$$

A receptor has multiple binding sites and can exist in more than one conformational state, yielding the general state diagram represented in Scheme 1. According to this design, n represents the number of binding sites per receptor (Hill coefficient) and s the number of possible conformational transitions for each bound state (including the unbound or free one). Typically, the resting states are closed and the conformational transitions may be to closed, open, or desensitized states. As an example, the enclosed region (*dashed lines*) represents a two-step binding reaction with two possible conformations for each bound state. In this case, the resting states (R, AR, and A_2R) are closed and the transitions are to activated or open (R, AR, and A_2R_1). Some states may be inaccessible, if the kinetic rates that lead to them are set to zero.

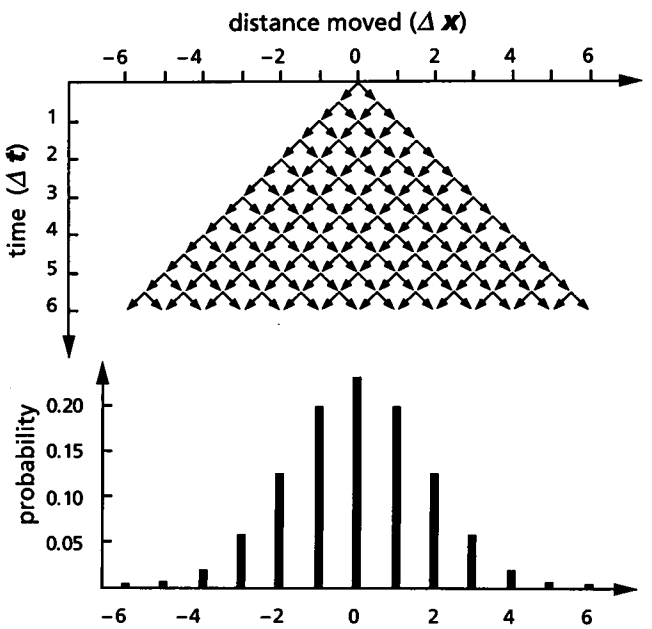

FIGURE 2 Random walk method of diffusion simulation. Movements of each transmitter molecule are simulated separately from other molecules, with movements in the x and y directions being independent of each other. Note that the diffusion time step, Δt, encompasses two half steps and two "half movements," which are a purely mathematical construct designed to achieve a Gaussian distribution after several time steps. The top diagram shows all possible positions (*abscissa*) a molecule can reach during a series of six short time steps (*ordinates*). The histogram below represents the binomial probability distribution of total distance moved in that time.

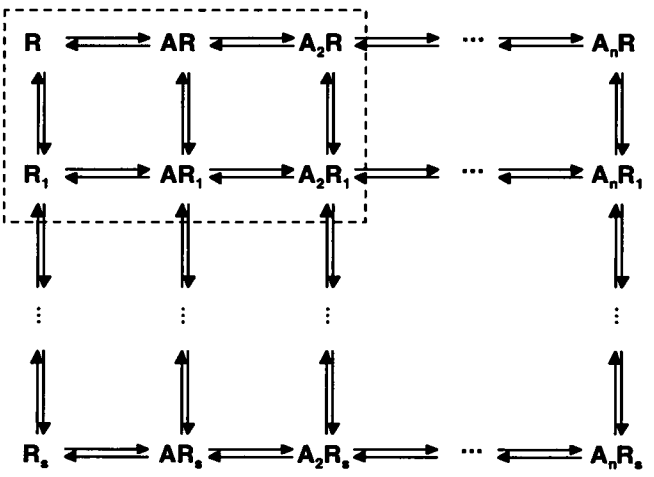

Scheme 1 A, agonist or transmitter; R, receptor.

In the specific kinetic model used to obtain the majority of the results presented here (area outlined in Scheme 2), n = 2 and s = 1, such that each receptor has two binding sites. Thus, free and single- and double-bound receptors all have two possible conformational states, closed and open. However, the open states for the free and single-bound receptors were made inaccessible (N in Scheme 2), leaving only one open state (A_2R^*), as suggested by evidence that glycinergic IPSPs recorded from the Mauthner cell decay as a single exponential (Faber and Korn, 1980, 1982). Furthermore, use of a Hill coefficient of 2 is consistent with estimates obtained from the dose-response relation for the glycine-induced conductance increase in this neuron (Diamond and Roper, 1973; see Faber and Korn, 1978). However, since recent data from other systems suggest there may be three or even four binding sites per receptor (Akagi and Miledi, 1988,

Taleb and Betz, 1994; Bormann et al., 1993; Schmieden et al., 1989), the corresponding models were also tested.

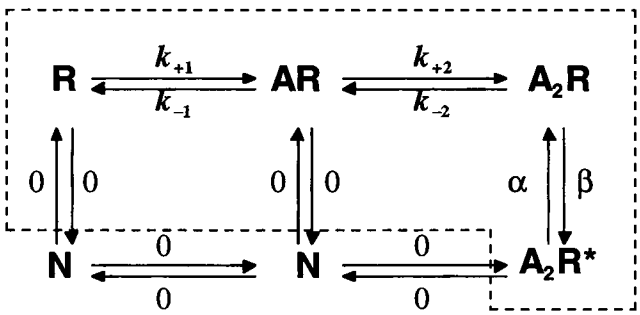

Scheme 2.

Simulation sequence

During each time step (δt) any free molecule that lands in a solid with a free or single bound receptor has a chance of binding to the latter. If it does bind, then it is flagged, and cannot move until it becomes unbound at some later time step. Similarly, every previously bound molecule may unbind. Since the chemical transitions are modeled by scanning the transmitter molecules once per δt, it is possible that a receptor will undergo multiple binding and/or unbinding reactions during that time step (maximally m reactions per receptor per δt). Each transmitter molecule, though, can undergo at most one binding or unbinding. A freshly unbound transmitter molecule will begin diffusing at the next time step. Finally, at the last phase of a time step, after all bindings and unbindings have occurred, each receptor may change its conformational state once.

The program generates waveforms of the number of receptors in the different states and the number of transmitter molecules in the cleft as functions of time, and the number of open channels is taken as a direct measure of the quantal current, also referred to as a mPSC. Examples of such results for single simulations are shown in Fig. 3. They illustrate the major characteristic that distinguishes Monte Carlo simulations from analytical solutions, namely "noisy" responses due to stochastic processes.

Analysis of the simulated data

Simulated mPSCs were fit with a double exponential function.

$$\mathrm{mPSC}(t) = b \times \left[\exp\left(\frac{-t}{\tau_d}\right) - \exp\left(\frac{-t}{\tau_r}\right)\right], \qquad (7)$$

where $\tau_d > \tau_r$. Typically, the decay time constant of the mPSC, τ_d, is an order of magnitude greater than the rise time constant, τ_r. The three parameters, b, τ_d, and τ_r were optimized using the method of least squares, and a weighting function $w(t) = t_{max}/(t + t_{max})$, where t_{max} is the first time at which the number of open channels is maximal. To facilitate comparisons with common experimental measures, we then calculated the time to peak, (t_p), as:

$$t_p = \frac{\tau_d \tau_r}{\tau_d - \tau_r} \ln\left(\frac{\tau_d}{\tau_r}\right) \qquad (8)$$

and we defined the peak amplitude, a, as the maximum number of open channels, which may or may not correspond to response amplitude at t_p. In this study, a is often expressed relative to the total number of available

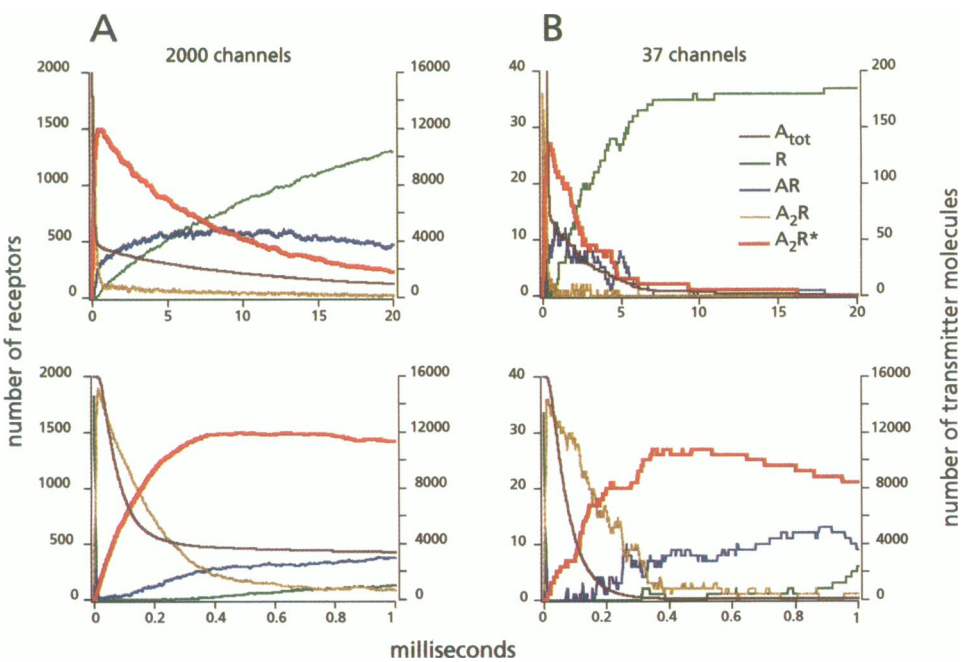

FIGURE 3 Simulated responses for large and small receptor matrices. (*A*) and (*B*), results of simulations with 2000 channels (density = 16,000 μm^{-2}) and 37 channels (density = 250 μm^{-2}), respectively. Other parameters identical for both: 16,000 transmitter molecules, r_{disk} = 200 nm, $r_{contact}$ = 400 nm, see Table 2 for kinetic parameters. Upper plots show the entire output (20 ms) while the details of the initial 1.0 ms are in the expanded curves below. The variables plotted are: the number of transmitter molecules (bound plus free) in the synaptic cleft (*purple*), and the numbers of receptors in the free (*green*), single bound (*blue*), double bound closed (*yellow*), and double bound open (*red*) states. Left and right ordinates represent receptors and transmitter molecules, respectively. The apparent noise in the plots can be attributed to the randomness of the simulation and is relatively greater for the simulation with fewer receptors.

channels, that is, in terms of the degree of saturation, S, with a value of 1.0 indicating 100% saturation (or all channels opened at the peak amplitude).

RESULTS

Single simulations

Examples of the outputs from two simulations are presented in Fig. 3. The two illustrated experiments only differed in receptor density, such that the number of receptors were 2000 and 37 in *A* and *B*, respectively. In both, the number of transmitter molecules released was appreciably larger, 16,000. This value is two to four times greater than estimates from both peripheral connections, such as the neuromuscular junction (Kuffler and Yoshikami, 1975), and from central synapses (e.g., calculated numbers for glutamatergic vesicles are only ~4000, Riveros et al., 1986). The upper plots show their full time courses, while the lower graphs are expanded representations of the initial 1 ms of each response. The numbers of receptors in different states and the number of transmitter molecules are all plotted versus time after release. In all cases, responses are "noisy," as is the time course of each state plot, and this feature is due to the stochastic properties of the chemical and conformational transitions. However, the stochastic "noise" is relatively larger when the postsynaptic matrix contains a small number of receptors, since it is proportional to the square root of this number while the response is directly proportional to it.

Most characteristics of the two simulated responses are quite similar, but others are clearly influenced by the difference in receptor numbers. For example, virtually no receptors are unbound (free) within 10 μs after exocytosis, and this condition persists for the first 0.5–1.0 ms. Also, the double-bound closed state is transitory, with the time to peak amplitude being ~0.35 to 0.4 ms for both simulations, and this parameter is primarily determined by the kinetics of the conformational transition. On the other hand, while the response of the matrix with the smaller number of receptors returns to the resting state within 7 to 10 ms, 35% of the receptors in the higher density cluster are still bound at 20 ms, reflecting a combination of buffered diffusion and the presence of a residuum of single-bound receptors (see below). Consequently, the response decays more slowly in larger clusters.

The time course of transmitter removal has two phases. There is an initial rapid decrease in the total number of molecules, representing the diffusional loss of free transmitter from the contact zone. For $r_{contact}$ = 400 nm and $D = 5 \times 10^{-6}$ cm^2 s^{-1}, the time constant of this process is ~0.1 ms (see also Clements, 1996). It is followed by a slower decay of the transmitter in the cleft, indicative of a delayed or buffered diffusion, because transmitter is bound to the receptors for milliseconds. The rate of this slow phase, determined by kinetics of receptor-transmitter interactions and by the number of receptors, can range from 3 to 20 ms, the longer value pertaining to larger receptor clusters.

Selecting adequate parameters

Kinetic constants

We first wished to simulate quantal glycinergic IPSPs recorded in the goldfish Mauthner cell soma, where initial estimates of quantal size ranged from 800 to 1200 or more open channels (Korn et al., 1982; Faber and Korn, 1982, 1988b). This value was based on an assumed single channel conductance of 25pS and needs to be reconsidered, given evidence for a dominant 40pS state for the glycine activated chloride channel in the M-cell of larval zebrafish (Legendre and Korn, 1994). Additional requirements extracted from the physiological results were a rise time of 0.3 to 0.4 ms (Faber and Korn, 1988b) and a decay time constant of ~6 to 10 ms (Faber and Korn, 1982). Also, as with other examples of fast synaptic transmission, the responses are mediated by a low affinity receptor, the apparent dissociation constant for glycine being of the order of 40 μM (Young and Snyder, 1973). Then, to simulate the responses of the adult M-cell, we first assumed the number of transmitter molecules was 10,000, and the receptor disk and contact zone were both quite large (r_{disk} = 0.23 μm, $r_{contact}$ = 0.5 μm), with a receptor density of 15,000/μm^2. The size of the contact zone is consistent with electron microscopic measurements of inhibitory synapses on the adult Mauthner cell soma (Triller and Korn, 1982), while that of the disk, which is somewhat larger than the postsynaptic density, was necessitated by the estimated quantal size (see Faber et al., 1985). These parameters were fixed, and we systematically varied the rate constants and diffusion coefficient to obtain an appreciation for the range of values that provided reasonable simulations. Generally, the model was run 10 to 20 times for a given parameter set. The results, summarized below, demonstrate that although various combinations provided satisfactory fits (see also Faber et al., 1992), the acceptable parameter space is circumscribed.

For most trials, k_{+1} and k_{+2} have been taken as 4×10^8 M^{-1} s^{-1}, which is close to the limit allowable by diffusion, and this choice dictated that k_{-1} and k_{-2} equal 16,000 s^{-1} to satisfy the requirement for a 40 μM dissociation constant. While it was possible to match a glycinergic IPSC with $D = 1.0 \times 10^{-5}$ cm^2 s^{-1}, β = 10,000 s^{-1}, and α = 500 s^{-1}, the range of parameters that provided adequate fits was quite narrow. For example, halving β slowed the rise time and accelerated the decay time constant by 25 to 33%. In general, parameter sets that gave an appropriately fast rate of rise tended to result in a response decay that was faster than that observed experimentally. We found that this deficiency was rectified by reducing k_{-1} an order of magnitude, to 1600 s^{-1}. This modification is consistent with the difference between the two unbinding rate constants derived for the acetylcholine receptor (Blount and Merlie, 1989), and it has the added consequence of keeping the number of single-bound receptors elevated during the response, as postulated previously (Faber and Korn, 1988a). This decreased rate of unbinding has two effects on the simulated responses, a slightly faster rate of rise and a slowed decay, and it in-

creases the range of parameters that provide adequate fits, namely β/α = 10 to 20:1 for $5000 < \beta \leq 15{,}000$ and $500 \leq \alpha \leq 1500$. To isolate the effects of structural parameters, the relevant simulations used a fixed set of rate constants, specifically: $k_{+1} = 4\times10^8\ M^{-1}\ s^{-1}$, $k_{-1} = 1600\ s^{-1}$, $k_{+2} = 4\times10^8\ M^{-1}\ s^{-1}$, $k_{-2} = 16{,}000\ s^{-1}$, $\beta = 5000\ s^{-1}$, and $\alpha = 500\ s^{-1}$.

It should be noted that we could not generate mIPSCs with the desired time course when α = 100 to 160 s^{-1}, which is the expected range for this rate constant if a channel opens at most once during a response with a mean open time of 6.7 to 10 ms (Faber and Korn, 1980, 1982). The higher values of α that were necessary imply that channels rather burst or flicker between states following exocytosis, and that was the case when the history of single channels was followed (Faber et al., 1992).

Diffusion constant

The diffusion constants for glycine and other small amino acids in the synaptic cleft are not known. We started with the assumption that it was fast, and asked if under that condition it was possible to simulate synaptic currents without invoking additional mechanisms for inactivating the transmitter or clearing it from the synapse. This approach was supported by experimental data showing that diffusion alone is sufficient at the M-cell's inhibitory synapses (Titmus et al., 1996) and for other central junctions (Clements et al., 1992; Dingledine and Korn, 1985; Hablitz and Lebeda, 1985; Hestrin et al., 1990). The model supported this perspective, and we then tested the effects of varying D, as the speed of diffusion could be expected to influence the degree of saturation and the extent to which a lateral spread of transmitter influences synaptic efficacy at neighboring junctions (Faber and Korn, 1988a; Isaacson et al., 1993). Halving the diffusion coefficient from 10^{-5} to 0.5×10^{-5} $cm^2\ s^{-1}$ slightly increased the probability of channel opening, such that the peak amplitude increased by 5 to 10%. However, the more dramatic effect was on response kinetics, as the peak time and decay time constant were both prolonged by 30 to 60%. We did not find any combination of rate constants that adequately fit the glycinergic IPSPs with $D < 0.5 \times 10^{-5}$ $cm^2\ s^{-1}$, and in the remaining sections, D was kept constant at that value.

Number of binding sites per receptor

Given the possible range of the Hill coefficient for the glycine receptor in vivo (see Methods), we explored the effect of increasing the number of binding sites to three, with only the triple-bound state being able to open. Simulations were done with all binding constants equal to $4 \times 10^8\ M^{-1}\ s^{-1}$, k_{-2} and $k_{-3} = 16{,}000\ s^{-1}$, and $k_{-1} = 16{,}000$ or $1600\ s^{-1}$. Interestingly, the consequences of adding an additional binding step were relatively minor. The peak amplitude decreased by only 5 to 10% and the responses were slightly faster, with the rise and decay times both accelerated, by ~10 to 20% and 15 to 33%, respectively. All three effects can be attributed to the increased likelihood of a single dissociation occurring when there are three binding sites rather than two, and multiple transitions between the fully liganded open and closed states.

Analysis of response variability

As mentioned, the Monte Carlo method allows one to explore the contribution(s) of the stochastic properties of the process being modeled to response variability. For that purpose, a simulation with a fixed set of parameters was run repeatedly and then the mean and standard deviation for A_2R^* (number of open channels) were calculated. We first asked whether variations in response amplitude, time to peak, and decay time were normally distributed, and all three could be fit by Gaussians. Thus, experimental distributions that are skewed, or non-Gaussian, presumably are indicative of additional sources of variability.

A more complete measure of response variability is the variance waveform, typically plotted against the mean in nonstationary fluctuation analysis to determine both 1) the number of channels in a membrane patch, and 2) single channel conductance (Sigworth, 1980). Although this method was first developed for the analysis of ionic currents activated by controlled voltage clamp command pulses, it has also been applied to mPSCs collected experimentally (Robinson et al., 1991; deKoninck et al., 1992; deKoninck and Mody, 1994; Traynelis et al., 1991–1993), where the stimulus is instead the transmitter that is released from a single vesicle and is rapidly cleared from the synapse. Theoretically, there should be a parabolic relation between the variance of recorded current (v) and the mean current waveform, allowing both single channel current, i, and the number, N, of functional channels to be estimated from the fit. Specifically, if all channels have the same probability of opening at any given time after release, the variance,

$$\mathbf{v} = i^2\left(\boldsymbol{u} - \frac{\boldsymbol{u}^2}{N}\right), \tag{9}$$

where u is the mean number of open channels. This would be the case if the transmitter concentration was homogeneous in the synaptic cleft throughout the duration of the responses. Since the model outputs channel numbers, $i = 1$ and the only unknown is N, we chose to assess the validity of this methodology, also used in a recent Monte Carlo simulation of hippocampal EPSCs (Wahl et al., 1996).

Fig. 4 compares the mean and standard deviation waveforms obtained from a series of 800 simulations with a fixed set of parameters. It illustrates a point stressed previously (Faber et al., 1992), namely that the intrinsic stochastic properties of the channels preclude complete saturation, already defined as 100% of the channels being open at the response peak (note, however, that functional saturation may be reached when all binding sites are occupied, even if not all channels are opened). Also, the standard deviation

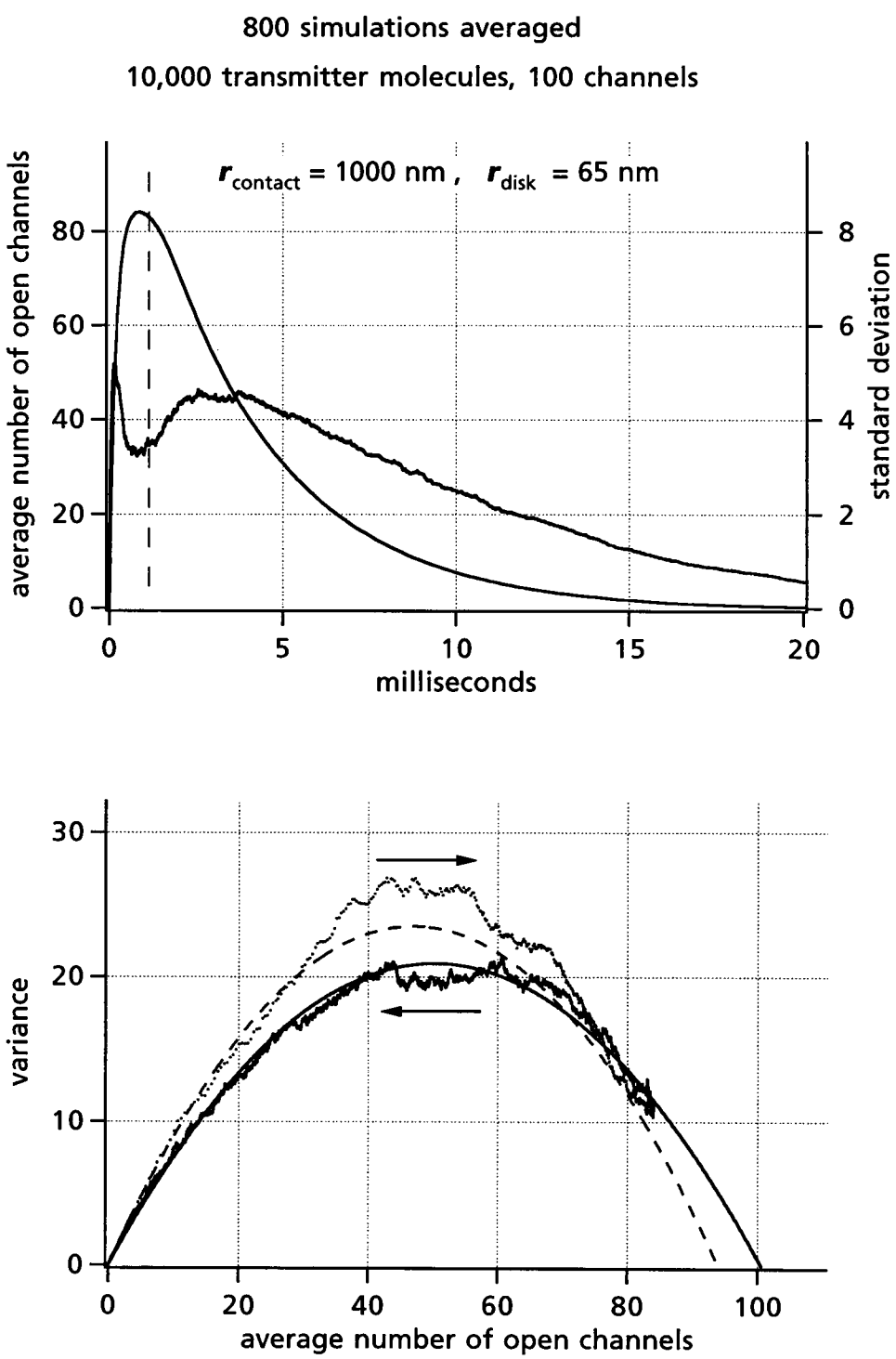

FIGURE 4 Nonstationary fluctuation analysis of simulated responses. *Top panel:* time course of the *average number of open channels* ($\bar{n}$) in a mPSC (*left ordinate*) and its standard deviation (σ, *right ordinate*); 800 individual mPSCs averaged. Note the local reduction in σ when >50% of the *total number of channels* (N = 100) available are open, e.g., at and around the peak of the response. *Bottom panel:* plot of instantaneous variance (σ^2) against instantaneous $-n$, and theoretical parabolas fit to this plot. Extrapolation of these parabolas to the second point of zero variance (abscissa intercept) allows estimation of N. Two parabolic fits are shown: $y = x - x^2/N$ (*dashed curve*), and $y = i^2(x - x^2/N)$ (*solid curve*). The latter is analogous to the experimental situation when both N and the single channel current (i) are unknown. The first fit underestimates N by 6% while the second better predicts N but underestimates i (see Table 1 and Discussion). The mean-variance scatterplot exhibits a hysteresis which indicates that the variance for equivalent values of $\bar{n}$ is greater during the rising phase of a mPSC (*upper arrow*) than during the falling phase (*lower arrow*). Receptor density, 7500 μm^{-2}. The data illustrated here are also represented in Table 1, bottom row.

waveform deviates from that of the mean, with maximal variance occurring on the rising and falling phases of the mPSC and there being a local minimum at its peak (Fig. 4, *top*). This dip indicates that the probability of channel opening is >50% at the peak, since the expected parabolic relationship implies a maximal variance when the opening probability equals 0.5. In confirmation, the plot of the variance versus the mean (Fig. 4, *bottom*), extends beyond the apogee of the parabola to a point where the peak amplitude corresponds to >80% of the channels open and the variance is about half its maximum.

Since the total number of channels was operator-defined, estimating the numbers of receptors from the mean-variance parabola might be expected to provide an independent validation of the model. However, when such a test was performed on several combinations of input parameters, chan-

TABLE 1 Estimates of the number of available channels from mean-variance (Sigworth) plots

No. of Transmitter Molecules	No. of Channels (N)	Estimated N (i = 1)	Error (i = 1)	Estimated N (i Variable)	Error (i Variable)	Estimated i	Saturation
			%		%		
500	61	42.9	−29.74	42.6	−30.23	1.00	0.3
1000	61	48.9	−19.79	52.8	−13.49	0.98	0.34
4000	61	48.9	−19.86	47.7	−21.80	1.01	0.36
16000	61	54.6	−10.45	60.9	−0.21	0.97	0.38
16000	47	38.4	−18.25	42.0	−10.54	0.97	0.4
8000	47	36.3	−22.79	34.4	−26.86	1.02	0.39
4000	47	31.1	−33.81	33.2	−29.31	0.97	0.38
2000	47	35.2	−25.15	39.9	−15.10	0.96	0.36
16000	47	47.3	0.68	49.1	4.57	0.97	0.8
16000	2000	1550	−22.50	2074	3.70	0.78	0.74
16000	37	37	0.00	39	5.41	0.97	0.71
16000	500	423	−15.40	550	10.00	0.82	0.73
8000	500	415	−17.00	461	−7.80	0.92	0.7
16000	300	270	−10.00	318	6.00	0.89	0.7
8000	300	265	−11.67	324	8.00	0.88	0.7
16000	101	96	−4.95	98	−2.97	0.98	0.72
8000	101	94	−6.93	96	−4.95	0.98	0.69
10000	101	94	−6.93	101	0.00	0.91	0.85

Kinetic parameters were as in Table 2, while the numbers of channels depended on both receptor disk radius and receptor density. All estimates were based on filtering mean-variance plots with Eq. 9, with i (single channel current) either fixed, equal to 1, or variable.

nel numbers were consistently underestimated. The results of 18 such experiments with 100 simulations each are summarized in Table 1. (The error was only slightly reduced when the number of simulations in a uniform series was increased to 800.) It indicates that in general, the higher the saturation the closer the prediction of this method was to the actual number of channels. Fig. 4, bottom also demonstrates that better fits could be achieved if i, the equivalent of single channel current, was not set equal to 1.0 but was allowed to be a free parameter (*dashed* versus *solid curves*). However, i was then underestimated. These discrepancies do not reflect errors in the model but are due to the fact that the time-dependent opening probability for a single channel depends upon its location in the postsynaptic matrix and presumably the concentration of transmitter it sees (see Discussion). Hence, criteria for applying Eq. 9 are not fulfilled.

Substrates for synaptic plasticity

Synaptic structure is plastic (Bailey and Kandel, 1993; Chen and Hillman, 1990; Hillman and Chen, 1985), with, for example, junctions going from being regions of flat apposition to concave or invaginated structures, as a function of prior activity (Desmond and Levy, 1986b; Fields and Ellisman, 1985; Fields et al., 1987; Petit et al., 1989). Also, the length of the contact zone is modifiable (Hillman and Chen, 1985; Chen and Hillman, 1990). We therefore tested the effects of several parameters: 1) contact zone radius, 2) number of receptor molecules, which is determined by receptor disk radius and surface density of the receptor molecules (see Methods: Receptor distribution), and 3) number of transmitter molecules released from a vesicle.

Their effects on three mPSC measures, namely the amplitude (a), time to peak (t_p), and decay time (τ_d) were quantified. Table 2 presents the ranges used for the parameter tested, and the values at which the others were kept constant. It can be noted that N, the number of receptors (channels) tested, varied between 37 and 2000.

For these experiments, simulations with each set of input parameters were repeated 16 times, the mPSCs averaged, and the average waveform fitted with the double exponential function (Eq. 7). Then the three measures were calculated as described in the Methods.

TABLE 2 Model input parameters

Parameter	Symbol	Value(s)
Diffusion constant	D	5×10^{-6} cm^2/s
Cleft height	h	0.02 μm
Contact zone radius	$r_{contact}$	0.05–1.6 μm
Receptor density	σ	250–16,000 μm^{-2}
Receptor disk radius	r_{disk}	0.025–0.2 μm
Receptor disk x position	x_{disk}	0 μm
Receptor disk y position	y_{disk}	0 μm
Vesicle release x position	$x_{vesicle}$	0 μm
Vesicle release y position	$y_{vesicle}$	0 μm
Number of transmitter molecules	A	250–16,000
Number of binding sites per receptor	n	2–3
Number of conformational transitions		1
First association rate	k_{+1}	4×10^8 M^{-1} s^{-1}
First dissociation rate	k_{-1}	1600 s^{-1}
Second association rate	k_{+2}	4×10^8 M^{-1} s^{-1}
Second dissociation rate	k_{-2}	16,000 s^{-1}
Channel opening rate	β	5000 s^{-1}
Channel closing rate	α	500 s^{-1}

Contact zone diameter

Analyses of synaptic plasticity typically focus on identifying accepted pre- or postsynaptic loci of action, such as changes in the probability of exocytosis, in the number of transmitter molecules released or of available receptors. We assessed the alternative possibility that modifying the contact zone radius would provide a structural mechanism that did not involve alterations in the above-mentioned factors. The consequences of this manipulation are shown in Fig. 5 where average mPSCs from two synapses with markedly different contact zone radii are compared. Specifically, the receptor-free annulus had a radius of 50 nm in one case and 400 nm in the other. With this extreme eightfold difference, the mPSC amplitude is significantly smaller for the less extensive contact zone, while its time to peak is shorter, and its decay time is longer. These two examples are taken from a more complete analysis, in which we tested the effect of contact zone radius for three combinations of other parameters:

r_{disk} (nm)	No. of Channels	σ (μm^{-2})
25	37	16,000
50	37	4,000
50	129	16,000

Each combination was simulated with 250, 2000, and 16,000 transmitter molecules. The results of all three sets are the same as those illustrated for the first combination (Fig. 6), with minor differences being a consequence of the different numbers of receptors (see next section).

Saturation and amplitude (which are proportional for a given parameter set) depended strongly on the size of the contact zone (Fig. 6, *top*). Regardless of the number of transmitter molecules, for 37 receptors in the disk, enlarging the radius of the contact zone from 100 to 800 nm resulted in an increased saturation, which then was relatively constant for larger annuli. That is, there is a sigmoidal relation between saturation and contact zone radius that can significantly alter synaptic efficacy without changes in the more

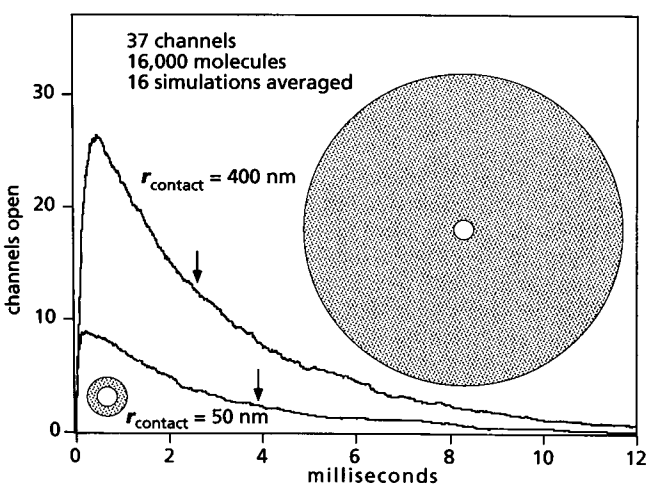

FIGURE 5 Effects of enlarging the contact zone. Plots of two averaged mPSCs (16 individual simulations in each) are shown for $r_{contact}$ = 50 nm and 400 nm, with all other geometrical, physical, and kinetic parameters kept constant. The contact zone sizes are illustrated by the gray disks (drawn to scale) surrounding the smaller concentric receptor disks (r_{disk} = 25 nm). The increased size of the contact zone resulted in a 200% increase in response amplitude, a doubling of peak time (0.51 vs. 0.22 ms), and an accelerated decay time constant (arrows at 2.6 and 3.9 ms). There were 37 channels in the disk, and 16,000 transmitter molecules. All other parameters as in Table 2.

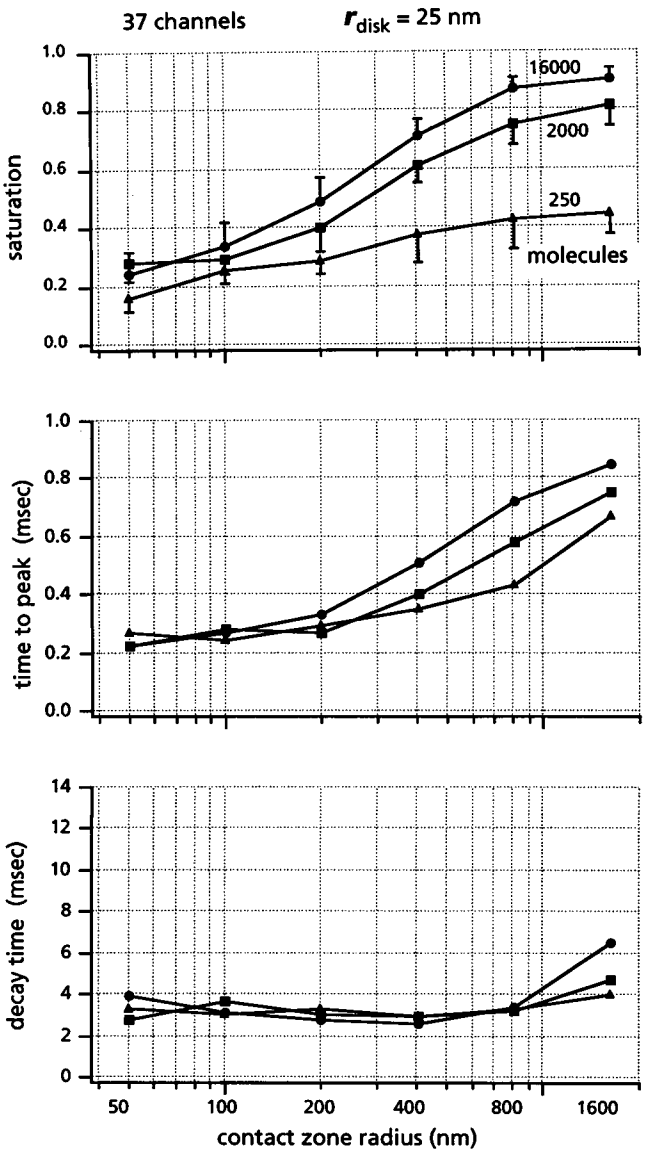

FIGURE 6 Quantitative relationships between contact zone radius and the mPSC amplitude and waveform. Three mPSC measures are plotted versus contact zone radius: saturation (*top*), time to peak (*middle*), and decay time (*lower*). The number of channels and their density were constant, and other parameters were as for Fig. 5, except for the number of transmitter molecules, which was 250 (*triangles*), 2000 (*squares*), or 16,000 (*circles*). For each data point, sixteen individual mPSCs were averaged, and the mean amplitude and its standard deviation (*error bars*) were measured at the peak of the resulting waveform, which was then fit with the double exponential function (Eq. 7) to calculate time to peak and decay time. Therefore, error bars for the two last variables could not be calculated.

classical determinants. When the number of receptors was increased to 129, the relationship was, as expected, shifted to the right (not shown). At the steepest regions of the sigmoid, doubling the contact zone radius from 200 to 400 nm increased response amplitude by 40%. The relation between contact zone radius and time to peak was equally striking (Fig. 6, *middle*), as doubling the radius produced a 20–50% increase in rise time.

These two effects of $r_{contact}$ presumably result from slower depletion of free transmitter from the larger contact zones, as opposed to its briefer availability in the smaller ones. The transmitter remains available approximately as long as it takes to diffuse to the edge of the synapse. With a higher initial number of transmitter molecules, a sufficient concentration in the synaptic cleft is also preserved for a longer period, so that the effects of transmitter amount and the contact zone size become synergistic. Consequently, the plots of contact zone radius versus saturation and time to peak are shifted to the left for higher numbers of transmitter molecules (Fig. 6, *top* and *middle*).

The other measurement parameter, decay time, is determined by the kinetics of channel closing, transmitter-receptor dissociation, and diffusion of the transmitter out of the synapse. Practically, this parameter remains relatively constant until the diffusion time approaches or exceeds the kinetic factors ($1/k_{-1}$, $1/k_{-2}$, and $1/\alpha$). Indeed, we observed that decay time was constant at ~3–4 ms until the contact zone radius exceeded 0.8 μm (Fig. 6, *bottom*), for which the diffusion time = 1.28 ms. Since the diffusion time is a function of the contact zone radius squared, it becomes the dominant component of the decay time for larger contact zones.

In summary, the contact zone radius proved to have a substantial effect on the mPSC amplitude, even if no kinetic parameters were altered. This effect may point to a previously unrecognized mechanism of plasticity in synaptic transmission that relies solely on simple changes in synaptic geometry and should be taken into consideration in interpreting the results of quantal analysis (Korn and Faber, 1991).

Number of channels and their distribution

Central synapses differ greatly in the number of their functional channels and in receptor density, as indicated by derived quantal sizes ranging from 10s to 100s of channels (Legendre and Korn, 1994; Faber and Korn, 1988b; Jonas et al., 1993; deKoninck and Mody, 1994; Traynelis et al., 1993; Robinson et al., 1991; Kraszewski and Grantyn, 1992). We therefore systematically varied the number of receptors in the postsynaptic membrane by using fixed geometrical parameters (e.g., r_{disk} = 200 nm and $r_{contact}$ = 400 nm), and varying the density of receptor packing from 250 to 16,000 μm^{-2}. The results are illustrated in Fig. 7, where saturation, time to peak, and decay time are plotted versus the number of channels.

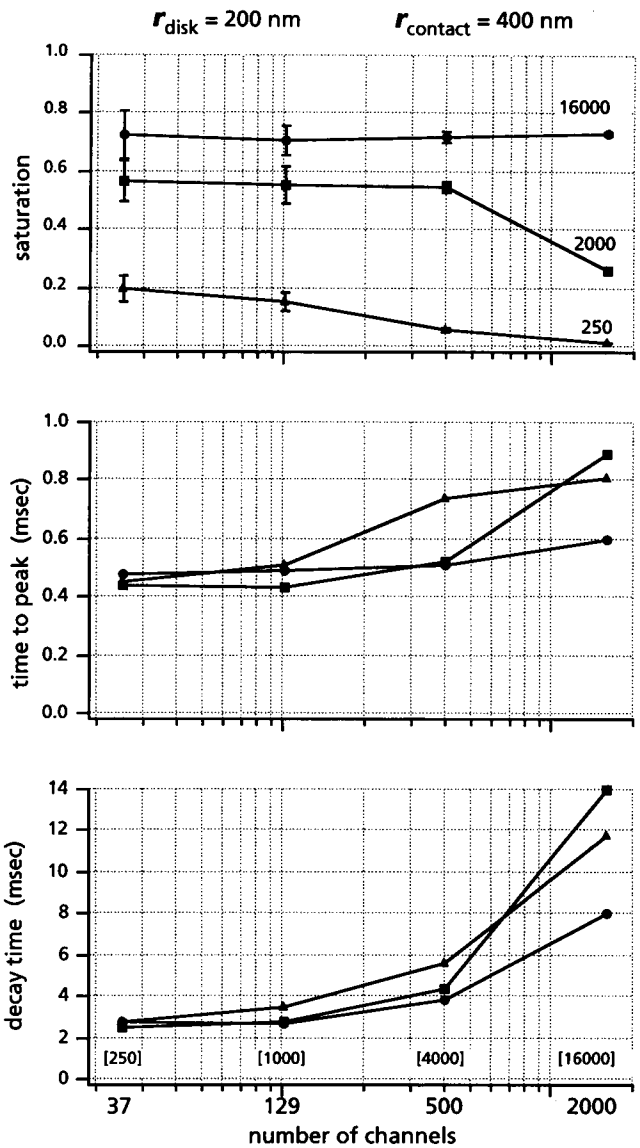

FIGURE 7 Effect of the number of available channels on mPSC characteristics. Similar format as in Fig. 6, but with abscissas indicating the total number of channels, varied by changing receptor density in a disk of fixed radius (200 nm). The bracketed numbers above the abscissa represent the corresponding surface densities expressed in channels/μm^2. Note that the number of channels is greater than calculated from the relationship: $N = \pi \times r_{disk}^2 \times \sigma$, since the algorithm can place receptors close to, or on, the edge of the disk (see Fig. 1 *D*). The number of transmitter molecules was 250, 2000, or 16,000, and all other parameters were kept constant ($r_{contact}$ = 400 nm). All other parameters as in Table 2.

First, for moderate numbers of transmitter molecules (250 and 2000), there was a reduction in saturation as the number of receptors increased from 37 to 2000 (Fig. 7, *top*). In contrast, if the number of transmitter molecules was large, 16,000, saturation remained constant at ~0.72. In this experiment, constant saturation indicates that response amplitude grows in proportion to the number of channels, which intuitively would only be expected for a large excess of transmitter relative to available binding sites. Further-

more, raising the number of receptors from 37 to 500 resulted in a mild growth in the time to peak (Fig. 7, *middle*) and decay time (Fig. 7, *bottom*). This slowing of the response kinetics was most pronounced when the number of receptors went from 500 to *2000*. Presumably, the prolongation is due to buffered diffusion which slows the removal of transmitter from the synaptic cleft. (It is not clear why the responses to 2000 transmitter molecules are slower than those to 1600 when the number of receptor is largest, 2000.) Increasing the number of receptors by holding their density constant and increasing the disk radius had similar effects on all three mPSC measures (not shown).

In the experiment of Fig. 8, the number of receptors was instead fixed to explore the consequences of varying their density, e.g., increasing density caused the receptor disk to shrink. This modification had at best a slight effect on saturation for the lowest number of transmitter molecules (250; Fig. 8, *top*) and did not alter either time to peak or decay time (Fig. 8, *middle, bottom*). Taken together, these results suggest that with a constant size of the surrounding contact zone, the crucial parameter that determines the amplitude, saturation level, and dynamics of a mPSC is the number of receptors, and not their distribution.

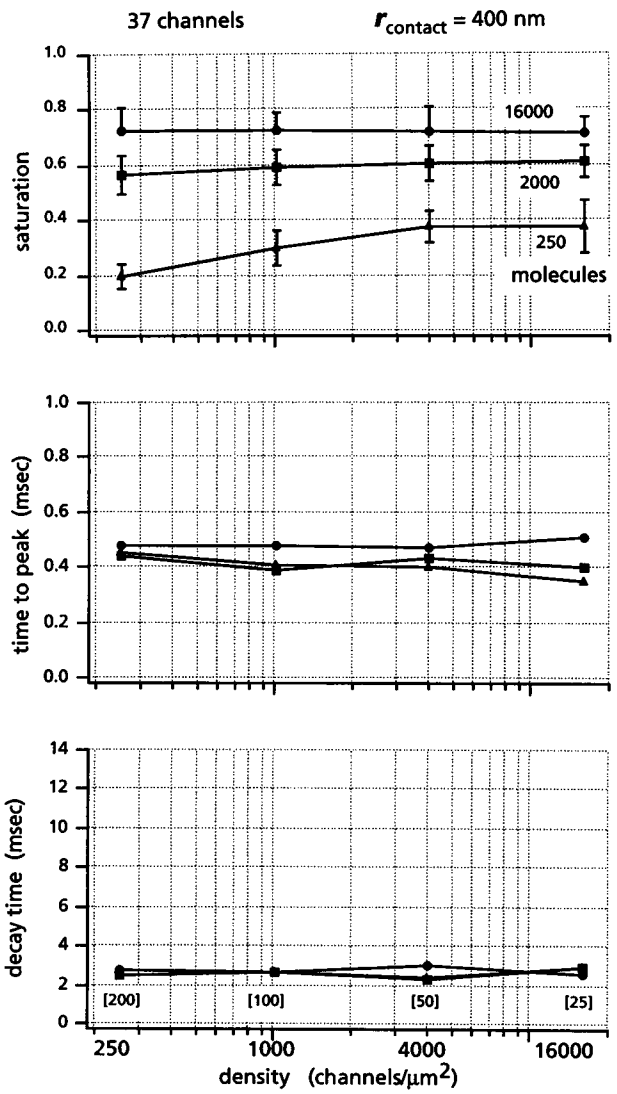

FIGURE 8 Relative insensitivity of mPSC properties to varying receptor density. Same presentation as in Figs. 6 and 7, but with a constant number of channels (37), obtained by varying density (*abscissa*) and disk radius (*bracketed value*) inversely. Note that the points for the highest density are common with those in Fig. 6 for $r_{contact}$ = 400 nm and those for the lowest density match values in Fig. 7 for 37 channels. All other parameters as in Table 2.

"Vesicle filling" and response parameters

One parameter that is not well defined at central synapses is the amount, A, of transmitter released per quantum. The vesicular concentrations of glycine and GABA are not known and estimates for glutamate range from 60 to 210 mM (Clements, 1996; Atwood and Wojtowicz, 1986), which would correspond to ~2000 to 8000 transmitter molecules per vesicle. Given this uncertainty, we initially explored the consequences of varying vesicular content from 200 to 20,000 molecules, with the number of receptors being as low as 5 and as great as 2000. In general, our results indicate that the degree of saturation varies in proportion to the vesicular content when A is less than 5 to 10 times the number of available receptors (or 2.5–5.0 times the number of binding sites) and becomes insensitive to this parameter when the ratio exceeds 20 (see Faber et al., 1992). Subsequently, rather than assume a large excess of transmitter molecules, we systematically used 250, 2000, and 16,000 transmitter molecules when exploring the effects of varying the different spatial parameters.

The effects on saturation of five different combinations of contact zone radius, disk radius, and number of receptors are shown in the bar plots of Fig. 9. Each parameter set was evaluated for the three different vesicular contents, and in each case saturation increased with vesicle filling. That is, as expected, the number of open channels at the peak of the response depends on transmitter concentration. This observation is consistent with theoretical predictions for the steady state. Saturation (S), which for our kinetic scheme is a sigmoidal function of concentration c, i.e.

$$S = \frac{[A_2R^*]}{N} = \left(\frac{k_{-1}k_{-2}\alpha}{k_{+1}k_{+2}\beta}\cdot\frac{1}{c^2} + \frac{k_{-2}\alpha}{k_{+2}\beta}\cdot\frac{1}{c} + \frac{\alpha}{\beta} + 1\right)^{-1} \quad (10)$$

Although an mPSC is a dynamic process far from steady state conditions, the basic sigmoidal characteristics of the transmitter concentration effect on saturation is preserved. That is, for 250 transmitter molecules, saturation is appreciably less than that for 2000 molecules, which in turn is less than that for 16,000, for all combinations tested.

The effects of the number of transmitter molecules on the two other measures of the mPSC, time to peak and decay time, were minor and probably not significant. The only exception was observed for large contact zones ($r_{contact}$ >

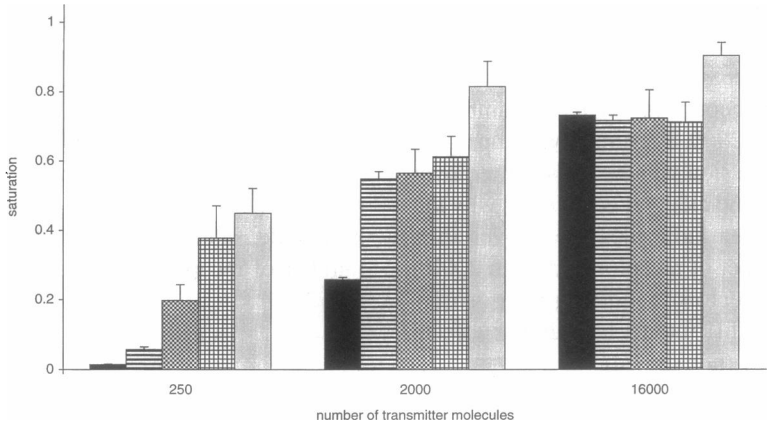

FIGURE 9 Effect of the number of transmitter molecules on saturation. Bar plots of saturation for five different combinations of *contact zone radius* ($r_{contact}$), *receptor disk radius* (r_{disk}), and *number of receptors* (N) for 250, 2000, and 16,000 transmitter molecules released. From left to right in each set:

1. $r_{contact}$ = 400 nm, r_{disk} = 25 nm, N = 2000 (*black bars*);
2. $r_{contact}$ = 400 nm, r_{disk} = 200 nm, N = 500 (*horizontal hatching*);
3. $r_{contact}$ = 400 nm, r_{disk} = 200 nm, N = 37 (*diagonal cross-hatching*);
4. $r_{contact}$ = 400 nm, r_{disk} = 250 nm, N = 77 (*horizontal* and *vertical bar hatching*);
5. $r_{contact}$ = 1600 nm, r_{disk} = 25 nm, N = 37 (*gray bars*).

Other parameters and calculation methods as in Fig. 6. Data presented here correspond to points selected from Figs. 6–8. Error bars = 1 SD.

400 nm) and a low number of receptors (37). In these conditions time to peak seemed to grow significantly with the number of transmitter molecules. With the maximum contact zone radius tested decay time also depended on vesicle content.

DISCUSSION

Stochastic models of postsynaptic currents at central synapses provide information concerning both the intrinsic variations or "noise" in the signaling process and the influence of specific kinetic or geometric parameters on the peak amplitude and time course of the responses. Although the initial goal of the present study was to simulate glycinergic synapses at the Mauthner cell of adult goldfish, where quantal size is quite large, the results may also pertain to other synapses having as few as five receptors (see also Faber et al., 1992). The speed of these responses, with rise times of 0.3 to 1.0 ms and decay time constants of 2–15 ms, is appropriate for a number of fast excitatory and inhibitory central synapses, although the kinetic models are different (Jonas et al., 1993; Busch and Sakmann, 1990).

Our results agree with those of Wahl et al., (1996) and previous analytical models (e.g., Faber et al., 1985; Land et al., 1984) that indicated that diffusion alone may be sufficient to rapidly remove neurotransmitter from the synaptic cleft. The range of diffusion coefficients used successfully, 0.5 to 1.0 $\times$ 10^{-5} cm^2 s^{-1}, encompasses those used in simulations of the neuromuscular junction and of central excitatory synapses. However, while there is agreement that slowing diffusion produces a small increase in peak amplitude and a pronounced slowing of mPSC decay, we found a significant effect on peak time that Wahl et al., (1996) did not. This difference might reflect the fact that their model treated the synaptic cleft as extending to infinity in the x and y directions while we incorporated a finite receptor-free annulus surrounding the receptor matrix. The larger diffusion space in their simulations presumably already increased peak times (Figs. 5 and 6) by allowing more transmitter to remain in the synaptic cleft, and reduced the sensitivity of this output parameter to changes in D.

Validity of the model

Presumably, the outputs generated by the diverse combinations of rate constants and spatial factors used in these simulations are not unique. However, they do provide realistic ranges for most parameters used, particularly since two different algorithms have been used to implement both diffusion and the scheme for transmitter-receptor interactions, with essentially the same results. Interestingly, we have chosen fast forward binding constants which are consistent with those derived for the nicotinic acetylcholine receptor at the neuromuscular junction (Auerbach, 1993; Blount and Merlie, 1989) but an order of magnitude faster than those estimated for non-NMDA glutamate receptors (Colquhoun et al., 1992; Jonas et al., 1993; Spruston et al., 1995), which also produce fast synaptic responses; yet, the ratios of the opening and closing rates are comparable. In the case of the glycine receptor, detailed single channel analysis of synaptic channels in the adult will be required to determine the appropriate kinetic scheme and to establish narrower limits on these rate constants.

The Sigworth (1980) plot of variance versus the mean number of open channels open has been used experimentally to estimate both single channel current and the number

of functional channels (deKoninck et al., 1992; deKoninck and Mody, 1993, 1994; Robinson et al., 1991; Traynelis et al., 1991, 1992), and in model simulations, to demonstrate that the data were comparable to the expected relation, which was generated by using the known number of channels (Wahl et al., 1996). A modification of this technique, known as the "peak-scaled nonstationary fluctuation analysis method" (Traynelis et al., 1993; Silver et al., 1996) scales the peak of each individual mPSC to the mean and estimates single channel current from the variance of the decay phase. We have asked whether the general approach used in most studies is appropriate for synaptic currents, and found that it is prone to errors, which can be large. The most likely explanation is that the assumption that all receptors have the same probability of opening at any point in time after exocytosis, which is implicit in the use of this analysis, is incorrect. Rather, since not all receptors are exposed to the same concentration of ligand (see also Uteshev and Pennefather, 1996), the probability of opening varies between them, probably as a function of their location in the disk. This explanation is consistent with the observation that the error was greatest for lower degrees of saturation, which signify smaller maximal open probabilities due to a lower transmitter concentration. The indication that the variance at peak amplitude is less than expected also supports this notion: the variance of a stochastic process is greater for a uniform process (simple binomial) than for one with unequal probabilities (compound binomial). Regardless, these results suggest that this method should be applied cautiously to experimental data, particularly if there is evidence for a low probability of channel opening at the response peak. For example, data that produced only the rising phase of the parabolic variance-mean plot would be one indication of an open probability <0.5.

The kinetics of exocytosis remain controversial, with estimates of the discharge time varying from as fast as 50 to 80 microseconds (Khanin et al., 1994; Stiles et al., 1996) up to 460 μs (Van der Kloot, 1995). We have adopted the simplifying assumption used in most other models (Land et al., 1981; 1984; Holmes, 1995; Wahl et al., 1996) of instantaneous release. On the other hand, Uteshev and Pennefather (1996) recently included noninstantaneous release in their mathematical description of mPSC generation, as well as "off-center" exocytosis. Both properties would increase the spatial inhomogeneity in transmitter concentration, and most likely in the probability of channel opening as well. Thus, noninstantaneous release would be another source of response variability.

It should be noted that in another model Holmes (1995) made the lateral extent of the contact zone sufficiently large such that further increases in this parameter would not affect the computed results, suggesting that smaller values artificially accelerated the removal of transmitter. However, that approach would make it impossible to consider the effect of the contact zone radius per se. In addition, the volume into which transmitter can diffuse increases significantly at the edge of most synaptic contacts, as there is some extracellular space between adjacent terminal endings on a postsynaptic cell (Peters et al., 1991). Thus, the approach of Holmes (1995) and the use of an infinite contact zone by Wahl et al. (1996) both preclude testing the effects of varying a potentially important geometric parameter. In our case, giving a transmitter molecule at the edge of the contact zone a 75% chance of remaining in the cleft is a reasonable compromise, as expansion of the diffusional space beyond that boundary could be expected to reduce the probability that a transmitter molecule reenter the central region where the receptors are clustered to nearly zero. Furthermore, the present scheme does not include a transmitter uptake mechanism, which would also accelerate the loss of transmitter if it were sufficiently fast.

Saturation

The idea of quantal saturation was first suggested on the basis of evidence that the peak amplitude of the derived quantal unit was invariant at the Ia afferent to spinal motoneuron connection in cat (Jack et al., 1981). Indeed, it was then postulated that complete saturation would be indicated by an invariant response with a standard deviation waveform equal to zero throughout the duration of the mPSC (Hirst et al., 1981). However, a more realistic expectation might have been a standard deviation waveform equal to zero when the mPSP is at its peak and with maxima on the rising and falling phases. Evidence for a local minimum in the variance waveform (Faber et al., 1992, 1995) is indicative that the degree of saturation exceeds 0.5, and that was often the case in the present study. The exceptions were when $r_{contact}$ was unusually small, for example 50 nm, such that most transmitter molecules escaped from the synaptic cleft before the majority of the receptors were double-bound (Figs. 5 and 6) or the numbers of molecules released and of available receptors were comparable (Fig. 7). Also, even when there was a large excess of transmitter molecules and the radius of the contact zone was significantly greater than that of the receptor cluster, saturation never reached 100%, and was typically $<80\%$. As described previously (Faber et al., 1992), this limitation occurs despite there often being 100% occupancy of the receptors: due to the stochastic properties of the channels it is highly unlikely that all double-bound receptor-channel complexes will be open at the same time. Specifically, the probability of this occurrence is $[\beta/(\alpha + \beta)]^N$, or 0.029 for 37 channels and 0.000007 for 125 channels. Consequently, peak amplitude will fluctuate from trial to trial, with a coefficient of variation that could be as low as 1% or as high as 25%. Typically, the smaller values pertained when saturation was $>50\%$ and there were at least a few hundred channels or when saturation was quite low, while the uncertainty in mPSC amplitude was greatest when few channels were involved. These relationships would be expected for a binomially distributed population.

While the arguments above indicate that saturation per se is unlikely, the insensitivity of response amplitude to in-

creased vesicle filling when there is already an excess of transmitter nevertheless indicates that responses characterized by 70 to 80% of the available channels opened at the peak may be functionally saturated. That is, quantal size will be maximal and insensitive to increased release. Then, postsynaptic mechanisms would be the best candidates for synaptic potentiation.

Consequences of altering geometric parameters

Structural changes in synapses have been associated with various types of synaptic plasticity, such as neuronal responses to injury and deafferentation (Chen and Hillman, 1990; Hillman and Chen, 1988) and as a substrate for long-term memory (Bailey and Kandel, 1993). These modifications include alterations in the geometry and size of the apposition between the pre and postsynaptic components (Bailey and Thompson, 1979; Desmond and Levy, 1983, 1986a,b, 1988; Petit et al., 1989; Temin, 1984, 1985); yet there has been no conceptual model that placed these changes in a functional perspective. The present results serve that purpose, as the most striking finding of the present set of simulations is that simply increasing the area of the receptor-free annulus surrounding the receptor cluster can increase peak amplitude and rise time, and, in extreme cases, prolong the decay phase. The most dominant effect is on amplitude, the common measure of synaptic strength. Furthermore, the range of contact zone radii that had significant effects, 0.2 to 2.0 μm, is similar to those observed morphologically at Mauthner cell synapses (Triller and Korn, 1982), and in higher structures such as hippocampus (Sorra and Harris, 1993; Spacek and Harris, 1997). Our results suggest that the size of the region in which the presynaptic terminal lies in opposition to the postsynaptic membrane is one parameter that should be carefully assessed in the future, and they provide a basis for the observation that the size of the contact zone at ribbon synapses of the ampullae of Lorenzini increases in parallel with synaptic efficacy (Fields and Ellisman, 1985, 1988; Fields et al., 1987). These contacts are flat and not very extensive at weak junctions, and they become invaginated, with a larger contact area, when synaptic strength is enhanced. Comparable changes might underlie modifications in the strength of synapses in other structures, where they would be manifest as an increased quantal size. Furthermore, an increase in quantal size is one of the mechanisms postulated to explain hippocampal long-term potentiation (Foster and McNaughton, 1991; Manabe et al., 1992), and it might be due, at least in part, to growth or expansion of the synaptic contact zone. These results, thus, reinforce the concept that the morphological properties of a synapse can significantly influence its function.

We thank William Young for his work on the earlier version of the model.

This work was supported in part by National Institutes of Health Grant NS21848 (to D.S.F.).

REFERENCES

Akagi, H., and R. Miledi. 1988. Heterogeneity of glycine receptors and their messenger RNAs in rat brain and spinal cord. *Science.* 242: 270–273.

Atwood, H. L., and J. M. Wojtowicz. 1986. Short-term and long-term plasticity and physiological differentiation of crustacean motor synapses. *Int. Rev. Neurobiol.* 28:275–362.

Auerbach, A. 1993. A statistical analysis of acetylcholine receptor activation in Xenopus myocytes: stepwise versus concerted models of gating. *J. Physiol. (Lond).* 461:339–378.

Bailey, C. H., and E. R. Kandel. 1993. Structural changes accompanying memory storage. *Annu. Rev. Physiol.* 55:397–426.

Bailey, C. H., and E. B. Thompson. 1979. Indented synapses in aplysia. *Brain Res.* 173:13–20.

Bartol, T. M., Jr., B. R. Land, E. E. Salpeter, and M. M. Salpeter. 1991. Monte Carlo simulation of miniature endplate current generation in the vertebrate neuromuscular junction. *Biophys. J.* 59:1290–1307.

Bekkers, J. M., G. B. Richerson, and C. F. Stevens. 1990. Origin of variability in quantal size in cultured hippocampal neurons and hippocampal slices. *Proc. Natl. Acad. Sci. USA.* 87:5359–5362.

Bekkers, J. M., and C. F. Stevens. 1995. Quantal analysis of EPSCs recorded from small numbers of synapses in hippocampal cultures. *J. Neurophysiol.* 73:1145–1156.

Blount, P., and J. P. Merlie. 1989. Molecular basis of the two nonequivalent ligand binding sites of the muscle nicotinic acetylcholine receptor. *Neuron.* 3:349–357.

Blum, K. L., and M. A. Idiart. 1994. A theoretical framework for quantal analysis and its application to long-term potentiation. *J. Neurophysiol.* 72:1395–1401.

Bormann, J., N. Rundstrom, H. Betz, and D. Langosch. 1993. Residues within transmembrane segment M2 determine chloride conductance of glycine receptor homo- and hetero-oligomers. *EMBO J.* 12:3729–3737.

Busch, C., and B. Sakmann. 1990. Synaptic transmission in hippocampal neurons: numerical reconstruction of quantal IPSCs. *Cold Spring Harbor Symp. Quant. Biol.* 55:69–80.

Chen, S., and D. E. Hillman. 1990. Robust synaptic plasticity of striatal cells following partial deafferentation. *Brain Res.* 520:103–114.

Clements, J. D. 1996. Transmitter timecourse in the synaptic cleft: its role in central synaptic function. *Trends Neurosci.* 19:163–171.

Clements, J. D., R. A. Lester, G. Tong, C. E. Jahr, and G. L. Westbrook. 1992. The time course of glutamate in the synaptic cleft. *Science.* 258:1498–1501.

Colquhoun, D., P. Jonas, and B. Sakmann. 1992. Action of brief pulses of glutamate on AMPA/kainate receptors in patches from different neurones of rat hippocampal slices. *J. Physiol. Lond.* 458:261–287.

deKoninck, Y., and I. Mody. 1993. Receptor saturation, channel kinetics and the applicability of nonstationary fluctuation analysis using simulation of quantal synaptic currents. *Soc. Neurosci. Abstr.* 19:1993.

deKoninck, Y., and I. Mody. 1994. Noise analysis of miniature IPSCs in adult rat brain slices: properties and modulation of synaptic $GABA_A$ receptor channels. *J. Neurophysiol.* 71:1318–1335.

deKoninck, Y., T. Otis, and I. Mody. 1992. Modulation of synaptic GABA currents in brain slices: nonstationary fluctuation analysis. *Soc. Neurosci. Abstr.* 18:401.

Desmond, N. L., and W. B. Levy. 1983. Synaptic correlates of associative potentiation/depression: an ultrastructural study in the hippocampus. *Brain Res.* 265:21–30.

Desmond, N. L., and W. B. Levy. 1986a. Changes in the numerical density of synaptic contacts with long-term potentiation in the hippocampal dentate gyrus. *J. Comp. Neurol.* 253:466–475.

Desmond, N. L., and W. B. Levy. 1986b. Changes in the postsynaptic density with long-term potentiation in the dentate gyrus. *J. Comp. Neurol.* 253:476–482.

Desmond, N. L., and W. B. Levy. 1988. Synaptic interface surface area increases with long-term potentiation in the hippocampal dentate gyrus. *Brain Res.* 453:308–314.

Diamond, J., and S. Roper. 1973. Analysis of Mauthner cell responses to iontophoretically delivered pulses of GABA, glycine and L-glutamate. *J. Physiol. Lond.* 232:113–128.

Dingledine, R., and S. J. Korn. 1985. Gamma-aminobutyric acid uptake and the termination of inhibitory synaptic potentials in the rat hippocampal slice. *J. Physiol. Lond.* 366:387–409.

Eccles, J. C., and J. C. Jaeger. 1958. The relationship between the mode of operation and the dimensions of the junctional regions at synapses and motor end-organs. *Proc. R. Soc. Lond. B. Biol. Sci.* 148:38–56.

Faber, D. S., P. G. Funch, and H. Korn. 1985. Evidence that receptors mediating central synaptic potentials extend beyond the postsynaptic density. *Proc. Natl. Acad. Sci. U.S.A.* 82:3504–3508.

Faber, D. S., and H. Korn. Editors. 1978. Neurobiology of the Mauthner Cell. Raven Press, New York. 290.

Faber, D. S., and H. Korn. 1980. Single shot channel activation accounts for duration of inhibitory postsynaptic potentials in a central neuron. *Science.* 208:612–615.

Faber, D. S., and H. Korn. 1982. Transmission at a central inhibitory synapse. I. Magnitude of the unitary postsynaptic conductance change and kinetics of channel activation. *J. Neurophysiol.* 48:654–678.

Faber, D. S., and H. Korn. 1988a. Synergism at central synapses due to lateral diffusion of transmitter. *Proc. Natl. Acad. Sci. USA.* 85: 8708–8712.

Faber, D. S., and H. Korn. 1988b. Unitary conductance changes at teleost Mauthner cell glycinergic synapses: a voltage-clamp and pharmacologic analysis. *J. Neurophysiol.* 60:1982–1999.

Faber, D. S., W. S. Young, P. Legendre, and H. Korn. 1995. Quantal fluctuations: correction. *Science* 270:1557.

Faber, D. S., W. S. Young, P. Legendre, and H. Korn. 1992. Intrinsic quantal variability due to stochastic properties of receptor-transmitter interactions. *Science.* 258:1494–1498.

Fields, R. D., and M. H. Ellisman. 1985. Synaptic morphology and differences in sensitivity. *Science.* 228:197–199.

Fields, R. D., and M. H. Ellisman. 1988. Functionally significant plasticity of synaptic morphology: studies on the ribbon synapse of the ampullae of Lorenzini. *Neuroscience.* 25:705–720.

Fields, R. D., M. H. Ellisman, and S. G. Waxman. 1987. Changes in synaptic morphology associated with presynaptic and postsynaptic activity: an in vitro study of the electrosensory organ of the thornback ray. *Synapse.* 1:335–346.

Foster, T. C., and B. L. McNaughton. 1991. Long-term enhancement of CA1 synaptic transmission is due to increased quantal size, not quantal content. *Hippocampus.* 1:79–91.

Frerking, M., S. Borges, and M. Wilson. 1995. Variation in GABA mini amplitude is the consequence of variation in transmitter concentration. *Neurology.* 15:885–895.

Hablitz, J. J., and F. J. Lebeda. 1985. Role of uptake in gamma-aminobutyric acid (GABA)-mediated responses in guinea pig hippocampal neurons. *Cell. Mol. Neurobiol.* 5:353–371.

Hestrin, S., P. Sah, and R. Nicoll. 1990. Mechanisms generating the time course of dual component excitatory synaptic currents recorded in hippocampal slices. *Neuron.* 5:247–253.

Hillman, D. E., and S. Chen. 1985. Compensation in the number of presynaptic dense projections and synaptic vesicles in remaining parallel fibers following cerebellar lesions. *J. Neurocytol.* 14:673–687.

Hirst, G. D. S., S. J. Redman, and K. Wong. 1981. Post-tetanic potentiation and facilitation of synaptic potentials evoked in cat spinal motoneurons. *J. Physiol.* 321:97–109.

Holmes, W. R. 1995. Modeling the effect of glutamate diffusion and uptake on NMDA and non-NMDA receptor saturation. *Biophys. J.* 69:1734–1747.

Isaacson, J. S., J. M. Solis, and R. A. Nicoll. 1993. Local and diffuse synaptic actions of GABA in the hippocampus. *Neuron.* 10:165–175.

Jack, J. J. B., S. J. Redman., and K. Wong. 1981. The components of synaptic potentials evoked in cat spinal motoneurons by impulses in single group Ia afferents. *J. Physiol.* 321:65–96.

Jonas, P., G. Major, and B. Sakmann. 1993. Quantal components of unitary EPSCs at the mossy fibre synapse on CA3 pyramidal cells of rat hippocampus. *J. Physiol. Lond.* 472:615–663.

Khanin, R., H. Parnas, and L. Segel. 1994. Diffusion cannot govern the discharge of neurotransmitter in fast synapses. *Biophys. J.* 67:966–972.

Korn, H., and D. S. Faber. 1991. Quantal analysis and synaptic efficacy in the CNS. *Trends Neurosci.* 14:439–445.

Korn, H., A. Mallet, A. Triller, and D.S. Faber. 1982. Transmission at a central inhibitory synapse. II. Quantal description of release, with a physical correlate for binomial n. *J. Neurophysiol.* 48:679–707.

Kraszewski, K., and R. Grantyn. 1992. Unitary, quantal and miniature GABA-activated synaptic chloride currents in cultured neurons from the rat superior colliculus. *Neuroscience.* 47:555–570.

Kruk, P. J., and D. S. Faber. Monte Carlo simulations of miniature synaptic currents suggest a structural mechanism for synaptic plasticity. *Biophys. J.* 68:A1.

Kuffler, S. W., and D. Yoshikami. 1975. The number of transmitter of transmitter molecules in a quantum: an estimate from iontophoretic application of acetylcholine at the neuromuscular synapse. *J. Physiol.* 251:465–482.

Land, B. R., W. V. Harris, E. E. Salpeter, and M. M. Salpeter. 1984. Diffusion and binding constants for acetylcholine derived from the falling phase of miniature endplate currents. *Proc. Natl. Acad. Sci. U.S.A.* 81:1594–1598.

Land, B. R., E. E. Salpeter, and M. M. Salpeter. 1981. Kinetic parameters for acetylcholine interaction in intact neuromuscular junction. *Proc. Natl. Acad. Sci.* 78:7200–7204.

Legendre, P., and H. Korn. 1994. Glycinergic inhibitory synaptic currents and related receptor channels in the zebrafish brains. *Eur. J. Neurosci.* 6:1544–1557.

Lewis, C. A., and D. S. Faber. 1996. Inhibitory synaptic transmission in isolated patches of membrane from cultured rat spinal cord and medullary neurons. *J. Neurophysiol.* 76:461–470.

Liu, G., and R. W. Tsien. 1995a. Properties of synaptic transmission at single hippocampal synaptic boutons. *Nature.* 375:404–408.

Liu, G., and R. W. Tsien. 1995b. Synaptic transmission at single visualized hippocampal boutons. *Neuropharmacology.* 34:1407–1421.

Manabe, T., P. Renner, and R. A. Nicoll. 1992. Postsynaptic contribution to long-term potentiation revealed by the analysis of miniature synaptic currents. *Nature.* 355:50–55.

Peters, A., S. L. Palay, and H. DeF. Webster. 1991. The Fine Structure of the Nervous System. Neurons and Their Supporting Cells. 3rd Ed. Oxford University Press, New York, Oxford.

Petit, T. L., J. C. LeBoutillier, E. J. Markus, and N. W. Milgram. 1989. Synaptic structural plasticity following repetitive activation in the rat hippocampus. *Exp. Neurol.* 105:72–79.

Press, W. H., S. A. Teukolsky, W. T. Vetterling, and B. P. Flannery. 1992. Numerical Recipes in C. Cambridge University Press, Cambridge.

Riveros, N., J. Fiedler, N. Lagos, C. Munoz, and F. Orrego. 1986. Glutamate in rat brain cortex synaptic vesicles: influence of the vesicle isolation procedure. *Brain Res.* 386:405–408.

Robinson, H. P. C., Y. Sahara, and N. Kawai. 1991. Nonstationary fluctuation analysis and direct resolution of single channel currents at postsynaptic sites. *Biophys. J.* 59:295–304.

Schmieden, V., G. Grenningloh, P. R. Schofield, and H. Betz. 1989. Functional expression in *Xenopus* oocytes of the strychnine binding 48 kd subunit of the glycine receptor. *EMBO J.* 8:695–700.

Sigworth, F. J. 1980. The variance of sodium current fluctuation at the node of Ranvier. *J. Physiol.* 307:97–129.

Silver, R. A., G. S. Cull-Candy, and T. Takahashi. 1996. Non-NMDA glutamate receptor occupancy and open probability at a rat cerebellar synapse with single and multiple release sites. *J. Physiol.* 494:231–250.

Sorra, K. E., and K. M. Harris. 1993. Occurrence and three-dimensional structure of multiple synapses between individual radiatum axons and their target pyramidal cells in hippocampal area CA1. *J. Neurosci.* 13:3736–3748.

Spacek, J., and K. M. Harris. 1997. Three-dimensional organization of smooth endoplasmic reticulum in hippocampal CA1 dendrites and dendritic spines of the immature and mature rat. *J. Neurosci.* 17:190–203.

Spruston, N., P. Jonas, and B. Sakmann. 1995. Dendritic glutamate receptor channels in rat hippocampal CA3 and CA1 pyramidal neurons. *J. Physiol. Lond.* 482:325–352.

Stibitz, G. R. 1969. Calculating diffusion in biological systems by random walks with special reference to gases diffusion in the lung. *Respiration Physiology.* 7:230–262.

Stiles, J. R., D. Van Helden, T. M. Bartol, Jr., E. E. Salpeter, and M. M. Salpeter. 1996. Miniature endplate current rise times less than 100 microseconds from improved dual recordings can be modeled with passive acetylcholine diffusion from a synaptic vesicle. *Proc. Natl. Acad. Sci. U.S.A.* 93:5747–5752.

Taleb, O., and H. Betz. 1994. Expression of the human glycine receptor α1 subunit in *Xenopus* oocytes: apparent affinities of agonists increase at high receptor density. *EMBO J.* 13:1318–1324.

Tieman, S. B. 1984. Effects of monocular deprivation on geniculocortical synapses in the cat. *J. Comp. Neurol.* 222:166–176.

Tieman, S. B. 1985. The anatomy of geniculocortical connections in monocularly deprived cats. *Cell. Mol. Neurobiol.* 5:35–45.

Titmus, M. J., H. Korn, and D. S. Faber. 1996. Diffusion, not uptake, limits glycine concentration in the synaptic cleft. *J. Neurophysiol.* 75: 1738–1752.

Traynelis, S. F., R. A. Silver, and S. G. Cull-Candy. 1991. Nonstationary current-variance analysis of glutamate receptor-mediated EPSCs at the mossy fiber-granule cell synapse. *Soc. Neurosci. Abstr.* 17:534.

Traynelis, S. F., R. A. Silver, and S. G. Cull-Candy. 1992. Estimated conductance of synaptic glutamate channels activated during EPSCs in rat cerebellar granule cells in thin slices. *J. Physiol. Lond.* 452:183P.

Traynelis, S. F., A. R. Silver, and S. G. Cull-Candy. 1993. Estimated conductance of glutamate receptor channels activate during EPSCs at the cerebellar mossy fiber granule cell synapse. *Neuron.* 11:279–289.

Triller, A., and H. Korn. 1982. Transmission at a central inhibitory synapse. III. Ultrastructure of physiologically identified and stained terminals. *J. Neurophysiol.* 48:708–736.

Uteshev, V. V., and P. S. Pennefather. 1996. A mathematical description of miniature postsynaptic current generation at central nervous system synapses. *Biophys. J.* 71:1256–1266.

Van der Kloot, W. 1995. The rise time of miniature endplate currents suggest that acetylcholine may be released over a period of time. *Biophys. J.* 69:148–154.

Wahl, L. M., C. Pouzat, and K. J. Stratford. 1996. Monte Carlo simulation of fast excitatory synaptic transmission at a hippocampal synapse. *J. Neurophysiol.* 75: 597–608.

Wathey, J. C. 1979. Numerical reconstruction of the quantal event at nicotinic synapses. *Biophys. J.* 27:145–164.

Young, A. B., and S. H. Snyder. 1973. Strychnine binding associated with glycine receptors of the central nervous system. *Proc. Natl. Acad. Sci. U.S.A.* 70:2832–2836.